Experimental study of one- and two-photon Rabi oscillations

Thomas R. Gentile, Barbara J. Hughey, and Daniel Kleppner
Research Laboratory of Electronics, Department of Physics, Massachusetts Institute of Technology, Cambridge, Massachusetts 02139

Theodore W. Ducas
Wellesley College, Wellesley, Massachusetts 02181
(Received 28 June 1989)

We report an experimental study of one- and two-photon Rabi oscillations and other coherent effects in microwave transitions between Rydberg states of calcium. Selective field ionization allows us to observe the time evolution of both the initial and final states with high discrimination. The experiments include measurements of the dependence of the one- and two-photon oscillation frequencies on microwave power and detuning from resonance. We have used the off-resonant behavior of the two-photon oscillation frequency to measure the ac Stark shift. In a magnetic field we have also observed the free evolution of the magnetic sublevels and the effect of Zeeman splitting on the one-photon Rabi oscillations. The theory for these experiments is presented; our results are in excellent agreement.

I. INTRODUCTION

The evolution of a two-level system subjected to a harmonic perturbation is a basic process in quantum mechanics. A characteristic feature is an oscillation in the populations of the two levels.[1] This behavior was first considered by Rabi[2] in the study of nuclear magnetic moments, hence the phenomenon is often referred to as a Rabi oscillation. In Rabi's original work and in subsequent magnetic resonance experiments, the interaction between magnetic moments and oscillating magnetic fields was studied.[3] With the advent of lasers, the interaction of two-level systems with optical radiation has been studied extensively.[4] In this regime, the term optical nutation is often used.

Simple oscillations in level populations can also be observed in multiphoton processes, and we will use the term Rabi oscillations for these phenomena in general. Since multiphoton processes usually require stronger radiation fields than one-photon processes, the ac Stark shift (power-dependent shift of the resonance frequency) can be an important effect. Two-photon Rabi oscillations have been observed by Hatanaka and Hashi[5] and Gold and Hahn,[6] and a variety of two-photon coherent effects have been studied theoretically[7–12] and experimentally.[13–14] The ac Stark shift has been observed in a two-photon process by Liao and Bjorkholm.[15] We have carried out a detailed experimental study of two-photon Rabi oscillations in Rydberg states of calcium, including measuring the ac Stark shift by examining the off-resonant behavior of the two-photon oscillation frequency. Only one intermediate state is important, and our results agree well with theory. We have also studied one-photon Rabi oscillations, whose well-known characteristics have provided a means for analyzing the systematics of our experimental system.

Realizing the optimal conditions for the study of Rabi oscillations requires two- or three-level systems that are free from radiative damping and a well-controlled interaction with the radiation. Such conditions are closely approximated by using microwave transitions between Rydberg states of calcium. We have nearly ideal two- or three-level systems because fine and hyperfine structure are absent in calcium singlet states. (The nuclear spin of the dominant isotope of calcium, ^{40}Ca, is zero.) The lifetimes of Rydberg states are long and the electric dipole-matrix elements between neighboring states are large. Consequently, a low level of microwave power can generate many Rabi oscillations in a time short compared to a lifetime, and so radiative damping is negligible.

Because the transitions are at microwave frequencies, the timing, strength, and frequency of the radiation field can be precisely controlled. The interaction occurs in a waveguide, in which the amplitude of the microwave electric field is constant for the duration of the interaction. The frequency of the Rabi oscillations, which depends on the electric field amplitude, is thus constant.

An additional advantage of Rydberg states is that selective field ionization can be used to detect and differentiate the initial and final states. This technique provides a simple and efficient method for observing the Rabi oscillations. The major disadvantage of Rydberg states is their sensitivity to electric fields; thus the control of stray electric fields is a challenge for this system.

Figure 1 shows a local-energy diagram for s, p, and d singlet states of calcium for principal quantum number $n \approx 50$. We have studied the $4snp\ ^1P_1 \rightarrow 4sns\ ^1S_0$ and $4snp\ ^1P_1 \rightarrow 4snd\ ^1D_2$ one-photon transitions, and the $4snp\ ^1P_1 \rightarrow 4s(n-1)p\ ^1P_1$ two-photon transitions. For the two-photon transitions it is possible for the $4s(n-1)d\ ^1D_2$ state to be the only important intermediate state, which allows us to study two-photon Rabi oscil-

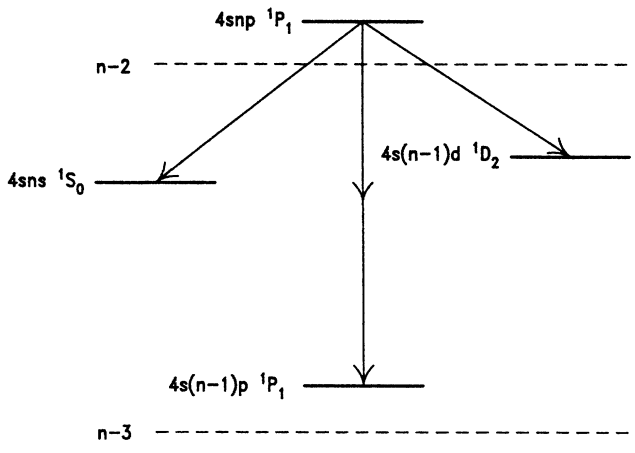

FIG. 1. Local-energy-level diagram for $n \approx 50$ showing the one- and two-photon transitions studied. The dashed lines indicate the locations of the $n-2$ and $n-3$ levels of hydrogen (levels with zero quantum defect).

lations in a simple three-level system. The two-photon transitions are driven with a single-frequency microwave source.

Section II provides a simple analysis of the behavior of one- and two-photon Rabi oscillations. The experimental apparatus is described in Sec. III. Section IV presents the results of our experiments on the power dependence and off-resonant behavior of the two-photon oscillation frequency and a study of the ac Stark shift. The theory of the ac Stark shift is developed in the Appendix. Section V presents the data and analysis of one-photon Rabi oscillations in a magnetic field, in which coherent effects between sublevels must be taken into account. Finally, possible extensions and applications of the research are discussed in Sec. VI.

II. THEORY

A. One-photon Rabi oscillations

The response of a two-level system to a harmonic perturbation is well known. We briefly review this topic to establish the notation and to aid the discussion of two-photon Rabi oscillations. Radiative damping is not important in our experimental system and therefore is neglected. Consider a system with two levels $|i\rangle$ and $|f\rangle$ with energies $\hbar\omega_i$ and $\hbar\omega_f$, respectively. We write the interaction Hamiltonian $W(t)$ in the form

$$\langle i|W(t)|f\rangle = \hbar\Omega_{if}\sin(\omega t) = \langle f|W(t)|i\rangle^* , \tag{1a}$$

$$\langle i|W(t)|i\rangle = \langle f|W(t)|f\rangle = 0 . \tag{1b}$$

We choose Ω_{if} to be real and time independent. An important parameter is the detuning from resonance, $\delta \equiv \omega - \omega_{if} \ll \omega_{if}$, where $\omega_{if} \equiv \omega_i - \omega_f$. The state of the system is expressed as

$$|\psi(t)\rangle = b_i(t)\exp(-i\omega_i t)|i\rangle + b_f(t)\exp(-i\omega_f t)|f\rangle , \tag{2}$$

and the time evolution of the coefficients $b_i(t)$ and $b_f(t)$ is obtained from Schrödinger's equation

$$\dot{b}_i(t) = -\tfrac{1}{2}\{\exp[i(\omega+\omega_{if})t] - \exp[-i(\omega-\omega_{if})t]\}\Omega_{if}b_f(t) , \tag{3a}$$

$$\dot{b}_f(t) = -\tfrac{1}{2}\{\exp[i(\omega-\omega_{if})t] - \exp[-i(\omega+\omega_{if})t]\}\Omega_{if}b_i(t) . \tag{3b}$$

For $\omega \approx \omega_{if}$ the terms proportional to $\exp[\pm i(\omega-\omega_{if})t]$ oscillate slowly, while the terms proportional to $\exp[\pm i(\omega+\omega_{if})t]$ oscillate much more rapidly. Because the time integral of the rapidly oscillating terms is nearly zero, these terms do not contribute significantly and therefore can be dropped (rotating-wave approximation). This approximation yields

$$\dot{b}_i(t) = \tfrac{1}{2}\exp(-i\delta t)\Omega_{if}b_f(t) , \tag{4a}$$

$$\dot{b}_f(t) = -\tfrac{1}{2}\exp(i\delta t)\Omega_{if}b_i(t) . \tag{4b}$$

We assume oscillatory solutions of the form

$$b_i(t) = B_i\exp(i\lambda t) , \tag{5a}$$

$$b_f(t) = B_f\exp[i(\delta+\lambda)t] , \tag{5b}$$

and obtain the two eigenvalues

$$\lambda_\pm = -\tfrac{1}{2}\delta \pm \tfrac{1}{2}(\delta^2+\Omega_{if}^2)^{1/2} . \tag{6}$$

If the system is initially in the state $|i\rangle$, then the time evolution of the populations is

$$|b_f(t)|^2 = \frac{\Omega_{R1}^2}{\Omega_1^2}\sin^2(\tfrac{1}{2}\Omega_1 t) , \tag{7a}$$

$$|b_i(t)|^2 = 1 - \frac{\Omega_{R1}^2}{\Omega_1^2}\sin^2(\tfrac{1}{2}\Omega_1 t) , \tag{7b}$$

where

$$\Omega_1^2 = \Omega_{R1}^2 + \delta^2, \quad \Omega_{R1} = \Omega_{if} . \tag{8}$$

We will refer to Ω_{R1} as the one-photon Rabi frequency and Ω_1 as the one-photon oscillation frequency. The populations of the states $|i\rangle$ and $|f\rangle$ oscillate at the frequency Ω_1. On resonance ($\delta=0$), the populations oscillate with unit amplitude at the Rabi frequency Ω_{R1}. As the radiation is tuned off resonance, the oscillations decrease in amplitude and increase in frequency. The full width at half maximum (FWHM) of the oscillation amplitude is twice the Rabi frequency Ω_{R1}.

In our experiments we study the interaction of an atom with monochromatic radiation with an electric field given by $\mathbf{E} = E_0\hat{\mathbf{z}}\sin(\omega t)$. The electric dipole interaction Hamiltonian is

$$W(t) = -\mathbf{d}\cdot\mathbf{E} = ezE_0\sin(\omega t) , \tag{9}$$

and so

$$\Omega_{R1}=\Omega_{if}=ez_{if}E_0/\hbar \ . \tag{10}$$

Here **d** is the electric dipole operator and $d_{if}=-ez_{if}$ is the electric dipole-matrix element between the two states $|i\rangle$ and $|f\rangle$. Thus the Rabi frequency for a one-photon transition is proportional to the amplitude of the electric field of the radiation.

B. Two-photon Rabi oscillations

Consider a three-level system with states $|i\rangle$, $|f\rangle$, and $|a\rangle$, as shown in Fig. 2. Radiative damping is again neglected. The interaction Hamiltonian can be written in the form

$$\langle i|W(t)|a\rangle=\hbar\Omega_{ia}\sin(\omega t) \ , \tag{11a}$$

$$\langle a|W(t)|f\rangle=\hbar\Omega_{af}\sin(\omega t) \ , \tag{11b}$$

$$\langle i|W(t)|f\rangle=0 \ , \tag{11c}$$

$$\langle i|W(t)|i\rangle=\langle f|W(t)|f\rangle=\langle a|W(t)|a\rangle=0 \ . \tag{11d}$$

For the states $|i\rangle$, $|f\rangle$, and $|a\rangle$ with unperturbed energies $\hbar\omega_i$, $\hbar\omega_f$, and $\hbar\omega_a$, respectively, we define $\omega_{if}\equiv\omega_i-\omega_f$, etc. As shown in Fig. 2, the difference between the radiation angular frequency ω and the one-photon resonance frequency ω_{ia} is referred to as the "defect" $\Delta\equiv\omega-\omega_{ia}$. The detuning from the two-photon resonance is $\delta\equiv 2\omega-\omega_{if}=\Delta+(\omega-\omega_{af})$. (Note that with this convention a detuning of δ requires a change in the radiation frequency of $\frac{1}{2}\delta$.) Although the location of the intermediate state as shown in Fig. 2 corresponds to the real experimental system, the magnitude of the detuning has been exaggerated for clarity; in our experiments $\delta\ll\Delta$. If the state of the system is expressed as

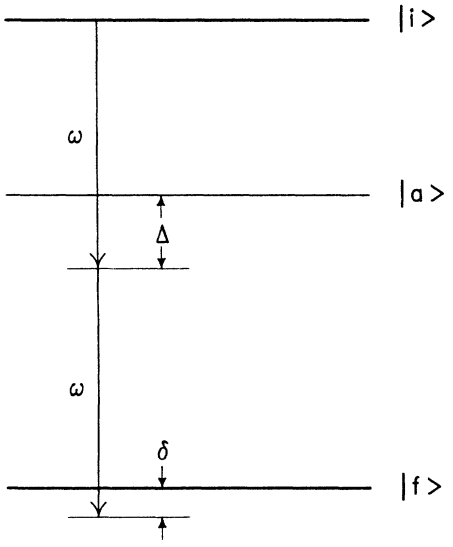

FIG. 2. Energy-level diagram for two-photon Rabi oscillations showing the microwave frequency ω, the defect Δ and the detuning δ. (The detuning is exaggerated for clarity.)

$$|\psi(t)\rangle=b_i(t)|i\rangle+b_a(t)|a\rangle+b_f(t)|f\rangle \ , \tag{12}$$

then the time evolution of the coefficients can be found from

$$\dot{b}_i(t)=-\tfrac{1}{2}\{\exp[i(\omega+\omega_{ia})t]-\exp[-i(\omega-\omega_{ia})t]\}\Omega_{ia}b_a(t) \ , \tag{13a}$$

$$\dot{b}_a(t)=-\tfrac{1}{2}\{\exp[i(\omega-\omega_{ia})t]-\exp[-i(\omega+\omega_{ia})t]\}\Omega_{ia}b_i(t) -\tfrac{1}{2}\{\exp[i(\omega+\omega_{af})t]-\exp[-i(\omega-\omega_{af})t]\}\Omega_{af}b_f(t) \ , \tag{13b}$$

$$\dot{b}_f(t)=-\tfrac{1}{2}\{\exp[i(\omega-\omega_{af})t]-\exp[-i(\omega+\omega_{af})t]\}\Omega_{af}b_a(t) \ . \tag{13c}$$

For $\omega\sim\omega_{ia}\sim\omega_{af}$, we can make the rotating-wave approximation and neglect the antiresonant terms $\exp[\pm i(\omega+\omega_{ia})t]$ and $\exp[\pm i(\omega+\omega_{af})t]$. With this approximation, we obtain

$$\dot{b}_i(t)=\tfrac{1}{2}\exp(-i\Delta t)\Omega_{ia}b_a(t) \ , \tag{14a}$$

$$\dot{b}_a(t)=-\tfrac{1}{2}\exp(i\Delta t)\Omega_{ia}b_i(t)+\tfrac{1}{2}\exp[-i(\delta-\Delta)t]\Omega_{af}b_f(t) \ , \tag{14b}$$

$$\dot{b}_f(t)=-\tfrac{1}{2}\exp[i(\delta-\Delta)t]\Omega_{af}b_a(t) \ . \tag{14c}$$

We assume solutions of the form

$$b_i(t)=B_i\exp(i\lambda t) \ , \tag{15a}$$

$$b_a(t)=B_a\exp[i(\lambda+\Delta)t] \ , \tag{15b}$$

$$b_f(t)=B_f\exp[i(\lambda+\delta)t] \ , \tag{15c}$$

and obtain the following cubic eigenvalue equation:

$$\lambda[(\lambda+\Delta)(\lambda+\delta)-\tfrac{1}{4}\Omega_{af}^2]-\tfrac{1}{4}\Omega_{ia}^2(\lambda+\delta)=0 \ . \tag{16}$$

The general solution is cumbersome. However, we can gain insight into the behavior of the eigenvalues by considering the case of resonance ($\delta=0$). For the resonant case we will label the eigenvalues λ_0, λ_+, and λ_-. For the general case ($\delta\neq 0$) we will label the eigenvalues λ_1, λ_2, and λ_3. The eigenvalues on resonance are

$$\lambda_0=0 \ , \tag{17a}$$

$$\lambda_\pm=-\tfrac{1}{2}\Delta\pm\tfrac{1}{2}(\Delta^2+\Omega_{ia}^2+\Omega_{af}^2)^{1/2} \ . \tag{17b}$$

Often, Ω_{ia}^2, $\Omega_{af}^2\ll\Delta^2$. This approximation will be satisfied if the probability of a one-photon transition to the intermediate state is negligible, as is true in our experiment. With this approximation,

$$\lambda_+\approx\frac{\Omega_{ia}^2+\Omega_{af}^2}{4\Delta}\equiv\Omega_0 \ , \tag{18a}$$

$$\lambda_-\approx-\Delta \ . \tag{18b}$$

Consequently, $\lambda_+\ll\lambda_-$. For small detunings, the eigenvalues are not expected to change significantly. Let us

consider the behavior of the large eigenvalue λ_3. Near resonance, $\lambda_3 \sim \lambda_- \gg \delta$, and $\lambda_3^2 \sim \lambda_-^2 \gg \Omega_{ia}^2, \Omega_{af}^2$. Applying these approximations to Eq. (16) yields $\lambda_3 \approx -\Delta$. For the two smaller eigenvalues (λ_0 and λ_+ on resonance) the cubic equation can be approximated by neglecting λ with respect to Δ. This leads to a quadratic eigenvalue equation:

$$\lambda^2+\lambda(\delta-\Omega_0)-\frac{\Omega_{ia}^2\delta}{4\Delta}=0 . \tag{19}$$

Therefore the conditions $\delta \ll \Delta$ and $\Omega_{ia}^2, \Omega_{af}^2 \ll \Delta^2$ lead to the following approximate solutions of the cubic eigenvalue equation

$$\lambda_1 \approx \tfrac{1}{2}(\phi-\Omega_2) , \tag{20a}$$

$$\lambda_2 \approx \tfrac{1}{2}(\phi+\Omega_2) , \tag{20b}$$

$$\lambda_3 \approx -\Delta , \tag{20c}$$

where λ_1 and λ_2 are the solutions of Eq. (19) with

$$\phi \equiv \Omega_0-\delta , \tag{21a}$$

$$\Omega_2 \equiv [(\delta-\Omega_0)^2+\Omega_{ia}^2\delta/\Delta]^{1/2} . \tag{21b}$$

Note that as $\delta \to 0$, $\lambda_1 \to \lambda_0$, $\lambda_2 \to \lambda_+$, and $\lambda_3 \to \lambda_-$.

If the system is initially in the state $|i\rangle$, then by using the above approximations we obtain the time evolution of the populations

$$|b_f(t)|^2 \approx \frac{\Omega_{R2}^2}{\Omega_2^2}\sin^2(\tfrac{1}{2}\Omega_2 t) , \tag{22a}$$

$$|b_i(t)|^2 \approx 1-\frac{\Omega_{R2}^2}{\Omega_2^2}\sin^2(\tfrac{1}{2}\Omega_2 t) , \tag{22b}$$

$$|b_a(t)|^2 \approx 0 , \tag{22c}$$

where

$$\Omega_{R2}=\frac{\Omega_{ia}\Omega_{af}}{2\Delta} , \tag{23a}$$

$$\Omega_2^2=\Omega_{R2}^2+(\delta-\delta'_{if})^2 , \tag{23b}$$

$$\delta'_{if}=\frac{\Omega_{af}^2-\Omega_{ia}^2}{4\Delta} . \tag{23c}$$

As expected, the populations of the $|i\rangle$ and $|f\rangle$ states oscillate while the $|a\rangle$ state remains unpopulated. We will refer to Ω_{R2} as the two-photon Rabi frequency and Ω_2 as the two-photon oscillation frequency.

The two-photon oscillation frequency Ω_2 has been written in a form analogous to the expression for the one-photon oscillation frequency Ω_1. Once again, we consider an electric dipole interaction between the atom and monochromatic radiation polarized along the z axis. The one-photon Rabi frequencies are

$$\Omega_{ia}=ez_{ia}E_0/\hbar, \quad \Omega_{af}=ez_{af}E_0/\hbar . \tag{24}$$

While the one-photon Rabi frequency is proportional to the electric field amplitude (or to the square root of the power), the two-photon Rabi frequency [Eqs. (23a) and (24)] is proportional to the amplitude squared (and thus proportional to the power). The off-resonant behavior of the two-photon transition is identical to that of the one-photon transition except for a power-dependent shift of the resonance frequency δ'_{if}. This shift can be identified as the ac Stark shift of the two-photon transition. The particular expression for δ'_{if}, Eq. (23c), is only valid for a three-level system in the rotating-wave approximation. In real atomic systems, one must include the contribution from other levels. The general expression for the ac Stark shift of the two-photon transition is then

$$\delta_{if}=\left[\sum_s \frac{\Omega_{is}^2\omega_{is}}{2(\omega_{is}^2-\omega^2)}\right]-\left[\sum_s \frac{\Omega_{fs}^2\omega_{fs}}{2(\omega_{fs}^2-\omega^2)}\right] , \tag{25}$$

where the sum is over all intermediate states s and

$$\Omega_{jk}=ez_{jk}E_0/\hbar , \tag{26a}$$

$$\omega_{jk}=(E_j-E_k)/\hbar . \tag{26b}$$

This expression for the ac Stark shift is derived in the Appendix. The first term in Eq. (25) is the shift of the state $|i\rangle$ and the second term is the shift of the state $|f\rangle$. One can recover δ'_{if} from δ_{if} by restricting the sum to the three levels $|i\rangle$, $|a\rangle$, and $|f\rangle$ and using the approximation $\omega_{ia}(\omega_{ia}^2-\omega^2)^{-1} \approx \omega_{fa}(\omega_{fa}^2-\omega^2)^{-1} \approx -\frac{1}{2}\Delta$. Note that the shift is linearly proportional to the power.

Measuring the slope of the power dependence of the ac Stark shift requires an absolute microwave power measurement, which is difficult. However, if δ_{if} is expressed in terms of the two-photon Rabi frequency Ω_{R2} [Eq. (23a)], the explicit power dependence is eliminated. This provides an important advantage in our study of the ac Stark shift because we can measure the two-photon Rabi frequency with much higher accuracy than the absolute microwave power. Using Eqs. (23a), (25), and (26a), the expression for the ac Stark shift becomes

$$\delta_{if}=\Omega_{R2}\Delta\left[\left(\sum_s \frac{\omega_{is}}{\omega_{is}^2-\omega^2}\frac{z_{is}^2}{z_{ia}z_{af}}\right)-\left(\sum_s \frac{\omega_{fs}}{\omega_{fs}^2-\omega^2}\frac{z_{fs}^2}{z_{ia}z_{af}}\right)\right] . \tag{27}$$

C. Notation

Since all work described in this paper was done on singly excited calcium singlet states, the shorthand notation *np*, *ns*, and *nd* will subsequently be used in place of $4snp\ ^1P_1$, $4sns\ ^1S_0$, and $4snd\ ^1D_2$, respectively. All equations in this paper are expressed in SI units. The following list summarizes the notation for many of the frequencies that appear in this paper: Ω_{R1} is the one-photon Rabi frequency [Eq. (8)], Ω_1 is the one-photon oscillation frequency [Eq. (8)], Ω_{R2} is the two-photon Rabi frequency [Eq. (23a)], Ω_2 is the two-photon oscillation frequency [Eq. (23b)], $\Omega_{jk} \equiv ez_{jk}E_0/\hbar$ [Eq. (26a)] (assuming an electric dipole interaction), $\omega_{jk} \equiv (E_j-E_k)/\hbar$ [Eq. (26b)], Ω_B is the modified Rabi frequency [Eq. (30c)], and $\omega_L \equiv eB/2m_e$ is the Larmor frequency. In the dis-

cussion of the data we will often refer to frequencies in units of Hz: $\nu_x \equiv \Omega_x / 2\pi$. The frequencies ω_L and Ω_B are discussed in Sec. V.

III. EXPERIMENT

A schematic diagram of the apparatus is shown in Fig. 3. Rydberg atoms are produced by laser excitation in a thermal atomic beam of calcium. The atomic beam crosses a waveguide and then enters the detector, where selective field ionization is used to detect and differentiate the two Rydberg states involved in the transition. The laser excitation and subsequent interaction with microwave radiation both occur in the waveguide. We describe the experimental system, emphasizing those aspects that are essential to the experiment.

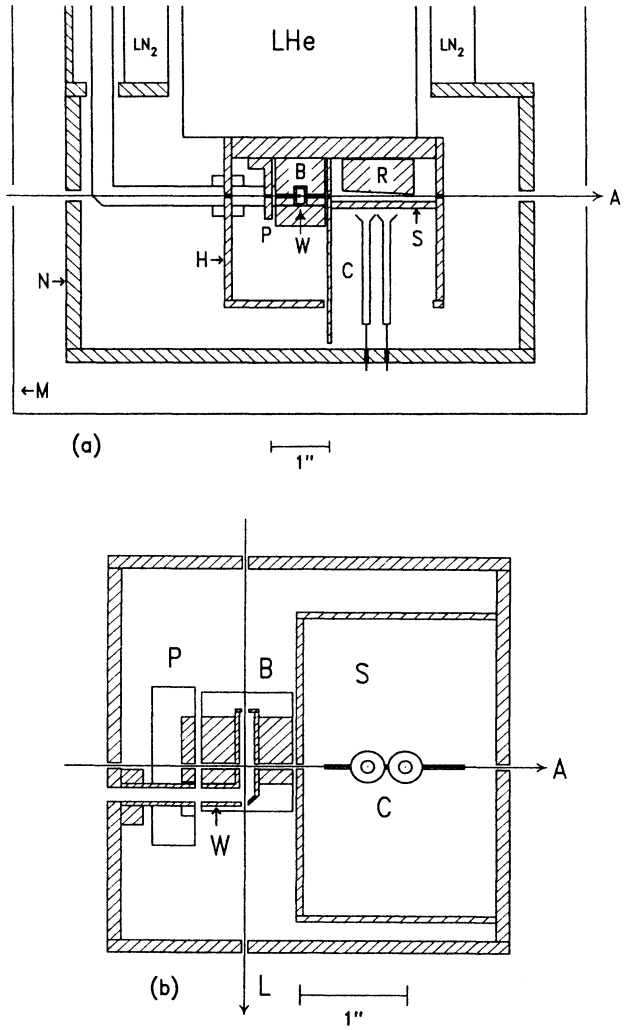

FIG. 3. Diagrams of the apparatus. (a) Side view of the system. *A*, atomic beam; *P*, collimating plate; *W*, waveguide; *B*, waveguide holder; *R*, ramped electric field plate; *S*, slotted electric field plate; *C*, channel electron multipliers; *H*, radiation shield connected to the liquid-helium reservoir; *N*, radiation shield connected to the liquid-nitrogen dewar; and *M*, magnetic shield. (b) View from below. *L*, laser beams.

A. Rydberg atom production

A calcium atomic beam is emitted from a "tube" oven operated typically at 500 °C. The beam passes through a collimating aperture and enters the waveguide where the laser excitation occurs. Rydberg states are produced by the three-step pulsed laser excitation scheme shown in Fig. 4. The second and third harmonics of a Nd:YAG (where YAG is yttrium aluminum garnet) laser (532 and 355 nm) are used to pump three grazing incidence dye lasers.[16] The 1034-nm light that drives the $4s4p \rightarrow 4s5s$ transition is produced in a KD*P (deuterated potassium dihydrogen phosphate) crystal that generates the difference frequency of a 525-nm dye laser and the Nd:YAG laser (1064 nm). By tuning the wavelength of the final laser, a wide range of $4snp$ Rydberg states can be excited. The results described here were obtained in the range $n = 45-52$. Unless otherwise noted, we shall take the quantization axis to be the direction of the microwave electric field, $\hat{z}$. With this convention, the selection rule for the microwave transitions is $\Delta m = 0$. ($m\hbar = \langle J_z \rangle$ where J is the total angular momentum.) The polarization of the final laser beam that drives the $4s5s \rightarrow 4snp$ transition can be selected with a half wave plate to be either parallel or perpendicular to $\hat{z}$. For parallel polarization the lasers populate the $m = 0$ sublevel of the np state; for perpendicular polarization a coherent superposition of the $m = +1$ and -1 sublevels is excited.

B. Microwave excitation

To study one- and two-photon Rabi oscillations quantitatively it is important to minimize averaging effects due to spatial or temporal variations in the microwave field.

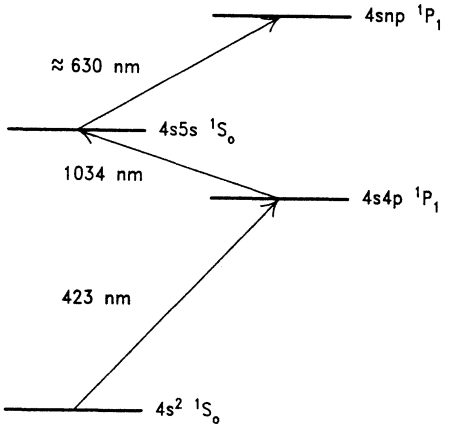

FIG. 4. Three-step pulsed dye-laser excitation scheme in calcium.

We have accomplished this by having the atoms traverse the waveguide along the direction in which the microwave electric field is constant, by exciting the atoms inside the waveguide, and by switching the microwaves on and off before a significant fraction of the atoms have left the waveguide.

The microwave radiation is ~ 30 GHz and is transmitted to the atoms through *WR*-28 waveguide (3.56×7.11 mm^2). As shown in Fig. 3(a), the atoms traverse the short axis of the waveguide, entering and leaving the waveguide through 1.3-mm apertures that do not significantly perturb the field. The collimating hole just before the waveguide restricts the atomic-beam diameter to 0.5 mm. The laser beams intersect the atomic beam 1.2 mm from the entrance, resulting in a mean transit time to the exit of 3 μsec; the interaction time with the microwaves is usually kept below 2 μsec.

Two techniques were used to define the characteristics of the microwave electric field at the atomic beam. In the first, the waveguide was shorted with a copper end cap to produce an antinode at the atomic beam. In this case the variation of the microwave field amplitude due to the finite width of the atomic beam is approximately 1%. This is the configuration shown in Fig. 3. The second method was to terminate the waveguide in a matched load so that the atoms interacted with a traveling wave. In this case the short was replaced by a bend and the load was located after this bend. The reason for this configuration is discussed in Sec. IV.

The microwave source is a 26.5–40-GHz sweep oscillator that is phase locked to a frequency synthesizer operated at approximately 1 GHz. Using a superconducting cavity with $Q > 10^7$ as a reference, we have verified that the short-term fluctuations in the microwave frequency are less than 400 Hz. The ~ 10-mW output of the sweep oscillator was attenuated 70–100 dB for studies of one-photon Rabi oscillations and 30–45 dB for two-photon Rabi oscillations, using a combination of fixed and variable attenuators. Since the power required for these transitions is extremely low, care is required to avoid spurious effects due to extraneous microwave power in the interaction region.

The interaction time of the atoms with the microwave radiation is varied by a computer-controlled pin diode microwave switch. The switch has 50-dB isolation, a rise time of 50 nsec, and a fall time of 5 nsec. The switch was opened immediately after the laser excitation and closed after a variable time period. The Rabi oscillations were observed by measuring the populations of the two Rydberg states for a range of microwave pulse lengths. Data was taken only for switch lengths greater than 200 nsec to avoid effects due to the rise time of the switch.

The range of Rabi frequencies we have measured extends from 0.4 to 12 MHz. Frequencies lower than 0.4 MHz were difficult to measure because the transit time of the atoms across the waveguide allowed less than one period of oscillation. Above 12 MHz, the resolution of the timing electronics limited the observations. We usually observed two to ten periods of oscillation, which allowed the Rabi frequencies to be extracted without complicated analysis.

C. Detector

The Rydberg atoms are observed with a two-channel field ionization detector that can monitor the individual populations of the two states with good state resolution. Rydberg atoms ionize in modest static electric fields (100 V/cm for the 46*p* state), and the Rydberg states involved in our transitions can be differentiated by the value of the electric field required for ionization. (This is not always possible: our observations are on $np \rightarrow ns$ rather than $np \rightarrow (n+1)s$ transitions because the np and $(n+1)s$ states ionize at nearly the same value of electric field). As the atoms emerge from the waveguide they pass between two electric field plates whose separation decreases linearly, which provides an increasing electric field. The ramp angle of these plates is chosen so that a single fixed voltage ionizes the two Rydberg states above their respective channel electron multipliers (CEM's). For a negative ramped plate voltage, the electrons released by the ionization pass through a slotted plate and are detected by one of the CEM's which generates an electrical pulse for each ionized atom. Consequently, we can count the number of atoms in both states involved in the transition. If all the population is in one state, the background signal on the CEM for the other state is about 4% of the total signal. This resolution can be obtained for a variety of transitions with a single ramp angle. The small background signal is due primarily to the finite resolution of selective field ionization.

D. Radiative transfer and spontaneous emission

The transfer between neighboring Rydberg states due to room-temperature blackbody radiation cannot be neglected because these transitions are at microwave frequencies and have large dipole-matrix elements. To reduce this undesirable effect, the apparatus is operated at liquid-nitrogen temperature or colder and is surrounded by a liquid-nitrogen cooled shield. With these precautions, radiative transfer is negligible.

To the best of our knowledge, there are no published measurements of the natural lifetimes of the Rydberg states used in these experiments. We estimate the *ns* and *np* lifetimes for $n \approx 50$ to be longer than ≈ 60 μsec based on scaling from available measurements[17,18] and our own observations. The lifetimes of the *nd* states are shorter, but these states are never populated [Eq. (22c)]. The neglect of radiative damping in Sec. II is therefore justified for these experiments because the mean transit time across the waveguide is only 3 μsec. The mean time from excitation to detection is 40 μsec, so less than $\approx 50\%$ of the Rydberg atoms decay before detection.

E. Effect of level splittings and broadening

Since the one- and two-photon oscillation frequencies are functions of the detuning from the atomic resonance frequency [Eqs. (8) and (23b)], the atomic response is affected by any perturbation that causes level splittings or broadening. Inhomogeneous broadening causes dephasing that washes out the Rabi oscillations. Splittings due to substructure can complicate the response of the system

(see Sec. V). The effective spectral half width of the atomic resonance is the Rabi frequency itself [Eqs. (7), (8), (22), and (23)], and so these effects can be neglected if the splittings or broadenings are small compared to the lowest Rabi frequency of interest. To assure that we observe at least one complete Rabi oscillation, we only study Rabi frequencies greater than the transit time linewidth of 300 kHz. We have reduced all splittings and broadenings to well under this value.

The use of a low-density atomic beam avoids collision broadening. Doppler broadening due to the longitudinal velocity distribution of the beam would be 100 kHz, but the actual broadening is negligible because the microwave radiation propagates transverse to the atomic-beam axis.

Effects of Zeeman splitting were reduced by employing a single-layer μ-metal magnetic shield and constructing the apparatus from nonmagnetic materials. The residual magnetic field in the waveguide of 5–10 mG causes a maximum splitting of 28 kHz between the $m=+1$ and -1 sublevels of an np state, which is less than 10% of the transit time linewidth. The effect of Zeeman splitting on the Rabi oscillations (Sec. V) was studied by removing the magnetic shield.

The Stark effect due to inhomogeneous stray electric fields is the most troublesome source of broadening in our experiments. These fields arise from a number of surface effects associated with the waveguide walls. The states we have chosen to study have no first-order Stark shifts in low fields because of their large quantum defects. However, the second-order Stark shift can still be significant. For example, in an electric field parallel to the quantization axis, the second-order Stark shift of the $46p \rightarrow 46s$ transition is 110 MHz/(V/cm)^2. The shift of the $46p \rightarrow 45p$ two-photon transition is more than an order of magnitude smaller because neighboring p states have nearly equal Stark shifts. With some difficulty, we reduced the stray electric field in the waveguide to 15 mV/cm. In this field the $46p \rightarrow 46s$ transition has a shift of only 25 kHz, and the shifts of the two-photon transitions are negligible. With the terminated waveguide the stray electric field was 85 mV/cm. However, this field was acceptable because it was fairly homogeneous. In addition, the work performed in this configuration was primarily studies of two-photon transitions.

F. Control of stray electric fields

The sources of stray electric fields and methods for reducing them deserve some additional discussion. We have found two major sources of these electric fields: surface contaminants and charge generation by laser photoionization. To reduce the latter, a resonant excitation scheme was employed which minimized the required laser power. Photoionization by the 423-nm laser out of the $5s$ state was further reduced by delaying the 1034-nm laser pulse relative to the 423-nm laser pulse.

The condition of the surface of the copper waveguide is important because the atoms are 1–2 mm from the waveguide surfaces while they interact with the microwave radiation. Our vacuum system is sealed with many large O rings and is pumped by an oil diffusion pump with a water cooled baffle. A mass analyzer has confirmed that the most prevalent contaminant is water. Our experience suggests that water on the waveguide surface results in stray electric fields as large as 0.5 V/cm. To reduce the partial pressure of water, we baked the entire vacuum chamber at 120 °C. The operating pressure was typically in the mid-10^{-8}-Torr range. The shield attached to the liquid-nitrogen reservoir was kept cold whenever the liquid-helium reservoir was cold so that it could cryopump outgassing water from the vacuum chamber. The calcium oven itself would sometimes cause a small increase in the electric field during a run. Cooling the apparatus with liquid helium greatly reduced this effect. The exact nature of this effect and its mysterious solution are not well understood, but similar behavior has been seen in another system.[19]

It was also found that if the powerful pulsed laser beams hit the edges of the entrance or exit holes of the waveguide, a stray electric field would be generated. This was presumed to be due to the ejection of contaminants or charge and their subsequent deposition on surfaces near the atom-microwave interaction region.

IV. RESULTS FOR TWO-PHOTON RABI OSCILLATIONS

The states relevant to the two-photon transition are shown in Fig. 5. For these experiments, the final laser is polarized perpendicular to the quantization axis, hence the $m=-1$ and $+1$ sublevels of the np state are equally populated. The ns states play no role in these two-photon transitions because of the $\Delta m=0$ selection rule on the microwave transitions. The analysis of Sec. II is valid because the $(n-1)d$ state is the only significant intermediate state. Since both the $m=-1$ and $+1$ sublevels are initially excited, there are two three-level systems evolv-

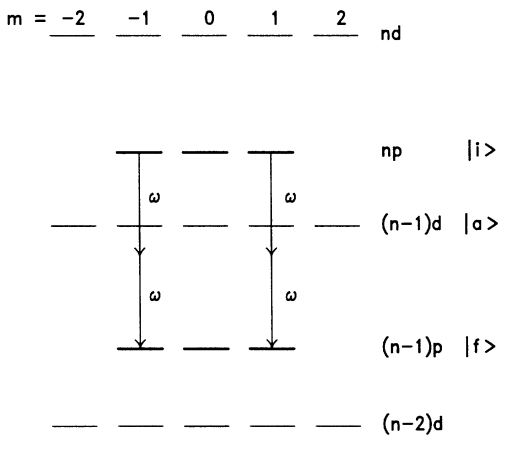

FIG. 5. Local-energy-level diagram for $n \approx 50$ showing all states involved in the two-photon Rabi oscillations. The laser excitation populates the $m=-1$ and $+1$ sublevels of the np state. The nd and $(n-2)d$ states contribute to the ac Stark shift only.

ing simultaneously. However, the relevant matrix elements are independent of the sign of m and the two systems are not coupled; therefore the problem can be treated as a single three-level system.

The ac Stark shift of a state is caused by its off-resonant coupling to nearby atomic levels by the radiation. Consequently, all transitions that are close to one-photon resonance can make large contributions to the ac Stark shift. The dominant contributions to the ac Stark shift of the $np \rightarrow (n-1)p$ two-photon transition are from the states nd, $(n-1)d$, and $(n-2)d$. We have accurately measured the transition frequencies to these states in another series of experiments.

In our experiments, the atoms interact with the microwave radiation in a rectangular waveguide operating in the fundamental (TE_{10}) mode. When the waveguide is terminated, the explicit expression for the one-photon Rabi frequency is

$$\Omega_{R1}=\Omega_{if}=\frac{ez_{fi}}{\hbar}\left[\frac{4P}{ab\epsilon_0 v_g}\right]^{1/2}, \tag{28}$$

where $a=7.11$ mm (long dimension of waveguide), $b=3.56$ mm (short dimension of waveguide), P is the microwave power, $v_g=c[1-(\lambda_0/2a)^2]^{1/2}$ is the group velocity in the waveguide, and $\lambda_0=2\pi c/\omega$.

The Rabi frequencies for a given microwave power can be calculated from Eq. (28) (one-photon) and Eqs. (23a) and (28) (two-photon). We have computed the radial matrix elements required for this calculation numerically;[20] a typical value is $n^2a_0 \approx 2500a_0$. Configuration interaction between the two valence electrons is not expected to affect these matrix elements at the level of accuracy required for comparison to our data. We have estimated the microwave power at the atomic beam by measuring the output power of the sweep oscillator and the attenuation and reflection characteristics of our waveguide system. Uncertainties in the measurements of the waveguide system limit the accuracy of this estimate of absolute power to $\pm 20\%$. We have calculated Rabi frequencies for various transitions from our computed matrix elements and microwave power measurements. These calculated Rabi frequencies are in agreement with our measured Rabi frequencies within the above experimental error (see Table I).

Figure 6 shows a two-photon Rabi oscillation of the $52p \rightarrow 51p$ transition. The horizontal axis represents the interaction time of the atoms with the microwave radiation, which is controlled by the microwave switch. The vertical axis is the number of atoms detected per laser pulse by the two CEM's. A summary of parameters for

TABLE I. Parameters of the $52p \rightarrow 51p$ Rabi oscillation shown in Fig. 6. The numbers in parentheses denote uncertainty in the last digit.

Transition frequency	$\omega_{if}/2\pi=53.88$ GHz
Defect	$\Delta/2\pi=6.76$ GHz
Computed matrix elements	$z_{ia}=3100a_0/\sqrt{5}$
	$z_{af}=2320a_0/\sqrt{5}$
Measured microwave power	$P=2.7(5)$ μW
Calculated Rabi frequencies	$\nu_{ia}=290(30)$ MHz
	$\nu_{af}=210(20)$ MHz
	$\nu_{R2}=4.5(9)$ MHz
Measured two-photon Rabi frequency	$\nu_{R2}=4.07(1)$ MHz

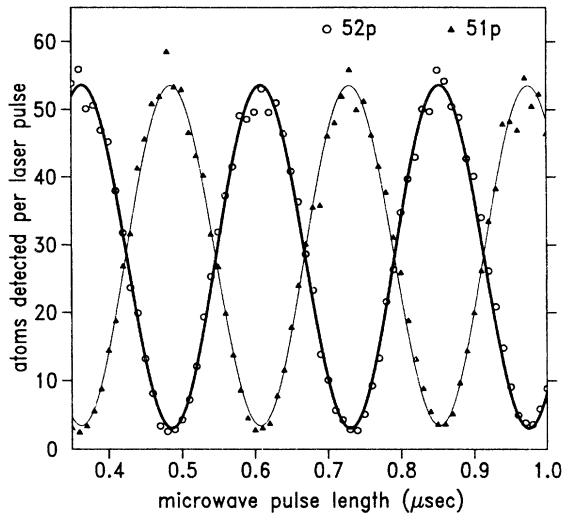

FIG. 6. Experimental results for the time evoluton of the $52p$ and $51p$ states undergoing two-photon Rabi oscillations. At the beginning of the plot (0.35 μsec), the system is starting its second oscillation. The solid curves are a fit of the data to a sinusoid.

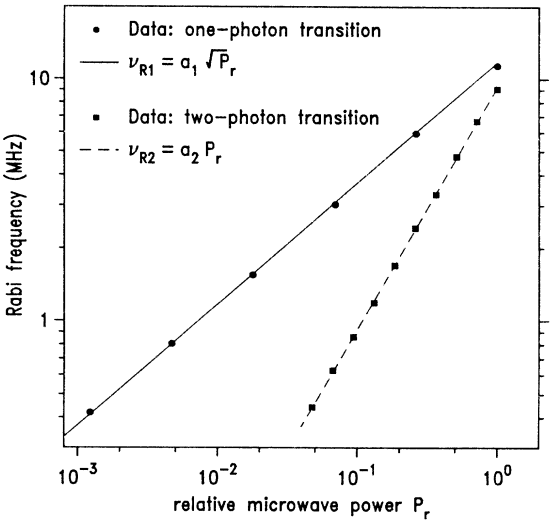

FIG. 7. Log-log plot of the variation of the one- and two-photon Rabi frequencies with the microwave power. As described in the text, ν_{R1} is proportional to the square root of the power and ν_{R2} is proportional to the power. The lines are fits of the data to these predicted power dependences; only the scale factors a_1 and a_2 are adjustable. The absolute power levels for the one- and two-photon transitions differ by a factor of $\approx 10^4$. The uncertainties in the data points are smaller than the size of the points.

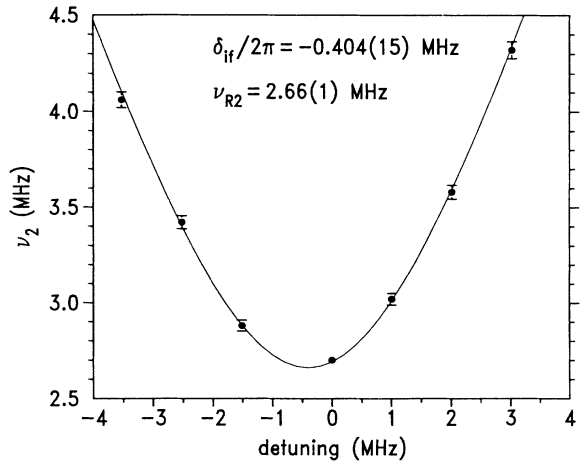

FIG. 8. Off-resonant behavior of the two-photon oscillation frequency ν_2 for the $46p \rightarrow 45p$ transition. The solid curve is a fit of the data to the expected form, Eq. (23b), that yields values for the ac Stark shift $\delta_{if}/2\pi$ and the two-photon Rabi frequency ν_{R2}.

the data in Fig. 6 is presented in Table I. It can be seen that the approximation $\Omega_{ia}^2, \Omega_{af}^2 \ll \Delta^2$ is excellent. The microwave radiation is at the ac Stark shifted resonance frequency, which requires a detuning of $\delta_{if}/2\pi = -0.56$ MHz at this power level.

Figure 7 shows the variation of the one- and two-photon Rabi frequencies with the microwave power on a log-log plot. The one-photon Rabi frequency is proportional to the square root of the microwave power [Eq. (28)], while the two-photon Rabi frequency is proportional to the microwave power [Eqs. (23a) and (28)]. The $46p \rightarrow 46s$ transition was used to obtain the one-photon data, and the $52p \rightarrow 51p$ transition was used to obtain the two-photon data.

Figure 8 shows the off-resonant behavior of the two-photon oscillation frequency ν_2 for the $46p \rightarrow 45p$ transition. The detuning δ is defined relative to the transition frequency we measured with the microwave power sufficiently low for the ac Stark shift to be negligible. It is experimentally impractical to detune much more than $\delta \approx 2\Omega_{R2}$ because the amplitude of the oscillations decreases off-resonance [Eqs. (22) and (23b)]. Therefore the approximation $\delta \ll \Delta$ is very good. As expected, the minimum oscillation frequency (ν_{R2}) does not occur at $\delta = 0$. A fit of the data to the expected form, Eq. (23b), yields values for the ac Stark shift $\delta_{if}/2\pi$ and the two-photon Rabi frequency ν_{R2}. This procedure was repeated at several power levels; the results are shown in Fig. 9. The data point near $\nu_{R2} = 0$ is from our transition-frequency measurement at low power as discussed above. A linear fit to the data yields the slope of the ac Stark shift versus the two-photon Rabi frequency [Eq. (27)]. We have repeated this entire procedure for four $np \rightarrow (n-1)p$ transitions; the results are shown in Table II. The calculated slopes were determined by using our measured transitions frequencies and computed matrix elements in Eq. (27). Only the nd, $(n-1)d$, and $(n-2)d$ states have been included in the calculation for each transition; including the other states would affect the result by less than 0.5%.

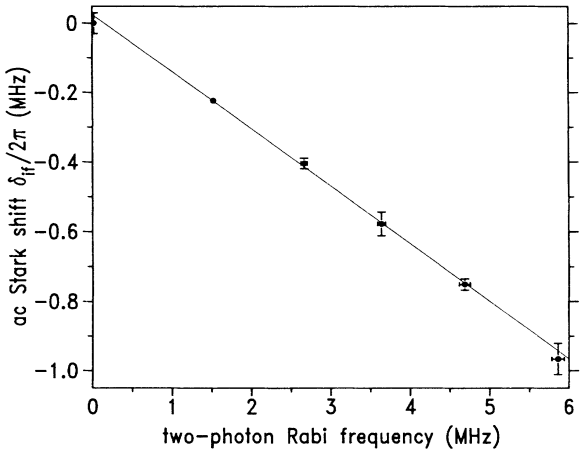

FIG. 9. The ac Stark shift $\delta_{if}/2\pi$ of the $46p \rightarrow 45p$ transition vs the two-photon Rabi frequency ν_{R2}. The solid curve is a fit of the data to the predicted linear dependence.

TABLE II. Measured and calculated slopes of the ac Stark shift vs two photon Rabi frequency δ_{if}/Ω_{R2}. The numbers in parentheses denote uncertainty in the last digit.

Transition	Measured slope	Calculated slope
$46p \rightarrow 45p$	0.165(12)	0.151
$48p \rightarrow 47p$	0.155(13)	0.141
$50p \rightarrow 49p$	0.134(13)	0.133
$52p \rightarrow 51p$	0.142(11)	0.126

As a check on the consistency of the measured slopes, we checked for shifts of various one-photon transitions. We do not expect to observe these shifts because they are much smaller than our experimental resolution. For example, the shift of the $46p \rightarrow 46s$ transition is calculated to be 2.4 kHz at $\nu_{R1} = 5$ MHz. However, when these experiments were first carried out using a shorted waveguide, power-dependent shifts were observed. These shifts were attributed to frequency-dependent reflections in the microwave system. In order to eliminate these reflections a matched load was installed at the end of the waveguide. In this case we observed no shifts of one-photon transitions within our experimental uncertainty. Consequently, we measured the shifts of the two-photon transitions with the waveguide terminated. The possibility of systematic power-dependent shifts smaller than our experimental resolution contributes an uncertainty of ± 0.01 in each of the measured slopes listed in Table II.

V. ONE-PHOTON RABI OSCILLATIONS IN A MAGNETIC FIELD

A magnetic field alters the dynamical behavior of the system. Although the two-level approximation is no longer valid, the magnetic sublevels evolve coherently

and this facilitates a detailed understanding of the response of the system. We have performed such a study in the ambient magnetic field in our laboratory. These experiments were performed on the $46p \rightarrow 46s$ transition. The analysis is particularly simple because the magnetic field is essentially perpendicular to the microwave electric field. We measured the magnetic field by observing the free evolution of the magnetic sublevels and also by scanning the microwave frequency over the atomic transition.

To analyze the evolution of the sublevels, consider a magnetic field $\mathbf{B}=B\hat{\mathbf{x}}$ perpendicular to the microwave electric field $\mathbf{E}=E_0\hat{\mathbf{z}}\sin(\omega t)$. In all of these magnetic field experiments, the microwave frequency is set at the resonance frequency for $B=0$ ($\omega=\omega_0$). We again choose the microwave electric field to be the quantization axis. In this experiment, the laser beams are polarized parallel to the microwave electric field, so only the $m=0$ sublevel of the $46p$ state is excited. A perpendicular magnetic field will cause a coherent evolution among the three magnetic sublevels. The evolution of the $46p$ state in the absence of microwave radiation can be expressed as

$$|\psi(t)\rangle = b_0(t)|0\rangle + b_{+1}(t)|+1\rangle + b_{-1}(t)|-1\rangle \ ,$$

where the $46p$ sublevels are labeled by the magnetic quantum number m. The evolution of the sublevels is found by diagonalizing the paramagnetic Hamiltonian $H=-\boldsymbol{\mu}\cdot\mathbf{B}=\omega_L L_x=\frac{1}{2}\omega_L(L_+ + L_-)$, where $\omega_L=eB/2m_e$ is the Larmor frequency. The populations of the magnetic sublevels are given by

$$|b_0(t)|^2=\cos^2(\omega_L t) \ , \tag{29a}$$

$$|b_{\pm 1}(t)|^2=\tfrac{1}{2}\sin^2(\omega_L t) \ . \tag{29b}$$

Note that all of the populations evolve at the frequency $2\omega_L$.

Figure 10 shows the free evolution of the magnetic sublevels of the $46p$ state. After laser excitation, the system evolves freely for a time T_D between 0 and 3 μsec, at which point the population is sampled by applying a short (30-nsec) microwave pulse. The power level of the microwaves is adjusted to drive the entire $46p$ $m=0$ population to the $46s$ state (π pulse). Atoms in the $46p$ $m=\pm 1$ states are unaffected because of the $\Delta m=0$ selection rule. Consequently, the microwave pulse probes the populations of the $46p$ sublevels at the instant it is applied. Atoms detected in the $46p$ state reflect the $46p$ $m=\pm 1$ population and atoms detected in the $46s$ state reflect the $46p$ $m=0$ population. The oscillations decrease in amplitude at long delay times because the mean transit time across the waveguide is 3 μsec. The $46s$ signal is smaller than the $46p$ signal because of the shorter lifetime of the $46s$ state. The period of the evolution in Fig. 10 corresponds to a magnetic field of 0.42 G.

To confirm the direction and magnitude of the magnetic field, we scanned the microwave frequency across the $46p \rightarrow 46s$ transition. The expected spectrum is best considered with a quantization axis along the magnetic field. In this case, the lasers excite a coherent superposition of the $m=-1$ and $+1$ states with both states equally populated. As shown in Fig. 11, two peaks are expected,

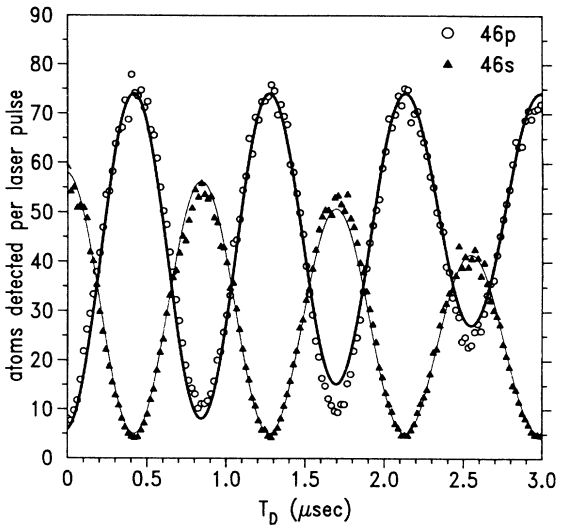

FIG. 10. Evolution of the magnetic sublevels of the $46p$ state sampled by population inversion, as described in the text. The solid curves are a fit of the data to the product of a sinusoid and an envelope function that takes into account the effect of atoms leaving the waveguide.

separated by $\Delta\omega=2\omega_L$. If the magnetic field were not perpendicular to the microwave electric field, however, there would be an $m=0$ to $m=0$ transition. We only observe two peaks, whose splitting confirms the value of the magnetic field determined from the free evolution experiment.

For our study of Rabi oscillations in a magnetic field it is again most convenient to choose the quantization axis along the magnetic field, as shown in Fig. 11. Three levels interact with the microwave radiation at frequency ω_0; the two allowed transitions are off resonance by $\delta=\mp\omega_L$

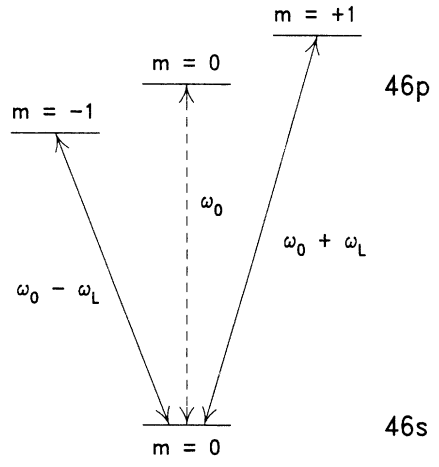

FIG. 11. Energy-level diagram for the $46p \rightarrow 46s$ transition with the quantization axis defined by the magnetic field. The transition frequency in zero magnetic field is ω_0; ω_L is the Larmor frequency.

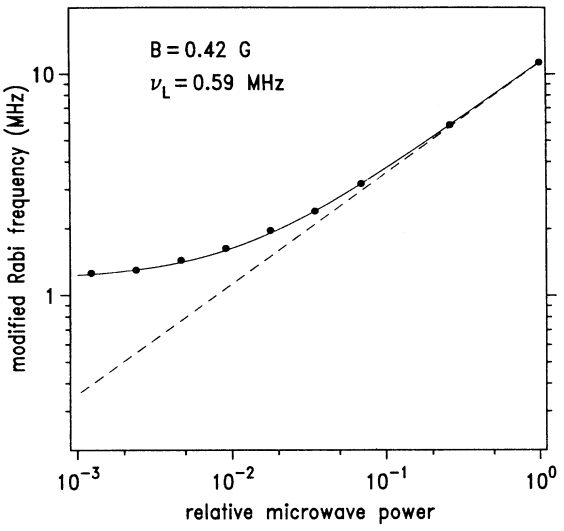

FIG. 12. The variation of the modified Rabi frequency ν_B with the microwave power. The solid line is a fit of the experimental data to the modified Rabi frequency [Eq. (30c)]. As in Fig. 7, the scale factor is the only adjustable parameter in the fit. Note that the modified Rabi frequency approaches $2\nu_L$ (1.18 MHz) at low power. The dashed line shows what the behavior would be in the absence of a magnetic field. The uncertainties in the data points are smaller than the size of the points.

($m=\pm 1$). Analysis of the three-level system yields the populations of the 46p (all magnetic sublevels) and 46s states

$$P(46p)=1-\frac{\Omega_{R1}^2}{\Omega_B^2}\sin^2(\tfrac{1}{2}\Omega_B t)\ , \tag{30a}$$

$$P(46s)=\frac{\Omega_{R1}^2}{\Omega_B^2}\sin^2(\tfrac{1}{2}\Omega_B t)\ , \tag{30b}$$

where

$$\Omega_B^2=\Omega_{R1}^2+4\omega_L^2\ . \tag{30c}$$

The populations oscillate at a modified Rabi frequency $\Omega_B=(\Omega_{R1}^2+4\omega_L^2)^{1/2}$, and the amplitude of the oscillation is Ω_{R1}^2/Ω_B^2. If $\Omega_{R1}\gg\omega_L$, the spectral width of the resonance is much greater than the Zeeman splitting and the transitions are both nearly on resonance. As expected, in this case Eq. (30) reduces to the solution for a two-level system on resonance. If $\omega_L\gg\Omega_{R1}$, the modified Rabi frequency approaches the frequency $2\omega_L$ and the amplitude is $\approx\Omega_{R1}^2/4\omega_L^2$. In this case, both transitions are far off resonance.

Figure 12 shows the observed variation of the modified Rabi frequency ν_B with microwave power on a log-log plot. The Larmor frequency is obtained from the measured period of the evolution of the magnetic sublevels (Fig. 10). Note that at low power the modified Rabi frequency approaches $2\omega_L$, as expected.

VI. CONCLUSION

Rydberg states undergoing microwave transitions constitute an excellent system for the study of the interaction of atoms with electromagnetic fields. The absence of fine and hyperfine structure in singlet states of alkaline earths provides a simple level structure. We have used calcium Rydberg states to study one- and two-photon Rabi oscillations and the ac Stark shift, and have obtained good agreement with theory. Our methods could be extended to the study of other coherent phenomena. Two-photon Rabi oscillations can be studied in regimes where the approximations fulfilled in our experiments are no longer valid. The large electric dipole matrix elements and convenient level structure of Rydberg states could make possible a study of three-photon Rabi oscillations. Our observation of the free evolution of the magnetic sublevels is a form of quantum beat spectroscopy. Possible applications of this technique to Rydberg states include the measurement of fine and hyperfine structure and the diagnosis of stray electric and magnetic fields. Finally, recent experimental studies of Rabi oscillations[21–24] and two-photon transitions[25] have been performed in the regime where the quantum nature of the electromagnetic field is important.

ACKNOWLEDGMENTS

This work was supported by the Joint Services Electronics Program under Grant No. DAAL03-89-C-0001. Earlier research was supported by the U.S. Office of Naval Research Grant No. N00014-79-C and the National Science Foundation Grant No. PHY84-11483.

APPENDIX: DERIVATION OF THE ac STARK SHIFT

We will calculate the ac Stark shift using a quantized electromagnetic field and a second quantized atom.[26] The advantage of this approach is that the atom-field interaction can be made time independent by transforming to the Schrödinger representation. This allows us to use time-independent perturbation theory instead of time-dependent theory[27] to calculate the ac Stark shift. We assume that the atoms interact with a single mode of the radiation field with no spatial variation along the atomic beam axis. We first consider the ac Stark shift of a two-photon transition, i.e., the case when the radiation is not resonant with any one-photon transition. The Hamiltonian is

$$H=H_A+H_F+H_{AF}\ , \tag{A1a}$$

$$H_A=\sum_k \hbar\omega_k|k\rangle\langle k|\ \ \text{(atom)}\ , \tag{A1b}$$

$$H_F=\hbar\omega(a^\dagger a+\tfrac{1}{2})\ \ \text{(field)}\ , \tag{A1c}$$

where $|k\rangle$ is an atomic eigenstate and $a^\dagger$ and a are the creation and destruction operators for the electromagnetic field mode with frequency ω. The atom-field interaction Hamiltonian in the electric dipole approximation is $H_{AF}=-\mathbf{d}\cdot\mathbf{E}$, where $\mathbf{d}=-e\mathbf{r}$. The dipole moment $\mathbf{d}$ can be expanded as

$$\mathbf{d}=\sum_{j,k}\mathbf{d}_{jk}|j\rangle\langle k| , \tag{A2}$$

where $\mathbf{d}_{jk}\equiv\langle j|\mathbf{d}|k\rangle$. The quantized electric field operator is given in the Schrödinger picture by

$$\mathbf{E}=\left[\frac{\hbar\omega}{2\epsilon_0 V}\right]^{1/2}\hat{\epsilon}(a+a^\dagger) , \tag{A3}$$

where $\hat{\epsilon}$ is the polarization direction and V is the volume of the "cavity" in which the field is quantized (periodic boundary conditions). Choosing the electric field along $\hat{\mathbf{z}}$ yields

$$H_{AF}=e\left[\frac{\hbar\omega}{2\epsilon_0 V}\right]^{1/2}\sum_{j,k}z_{jk}(a+a^\dagger)|j\rangle\langle k| . \tag{A4}$$

We will assume that the microwave radiation is a classical stable wave, i.e., that the field is in a coherent state $|\alpha\rangle$ with average photon number $\bar{n}=|\alpha|^2\gg 1$. The explicit expression for this coherent state in terms of the number states is

$$|\alpha\rangle=\exp(-\tfrac{1}{2}|\alpha|^2)\sum_n\frac{\alpha^n}{\sqrt{n!}}|n\rangle , \tag{A5}$$

where $|n\rangle$ is an eigenstate of the number operator $a^\dagger a$ with eigenvalue n. The actions of a and $a^\dagger$ on the number state $|n\rangle$ are given by $a|n\rangle=\sqrt{n}\,|n-1\rangle$ and $a^\dagger|n\rangle=\sqrt{n+1}|n+1\rangle$. The uncertainty in n is $\Delta n\ll\bar{n}$, so for the relevant number states, $n+\frac{1}{2}\approx n\approx\bar{n}\gg 1$. Assuming that the classical field varies as $\mathbf{E}=\mathbf{E}_0\sin(\omega t+\theta)$, we can make the correspondence

$$E_0=2\sqrt{\bar{n}}\left[\frac{\hbar\omega}{2\epsilon_0 V}\right]^{1/2} , \tag{A6}$$

and so H_{AF} becomes

$$H_{AF}=\frac{eE_0}{2\sqrt{\bar{n}}}\sum_{j,k}z_{jk}(a+a^\dagger)|j\rangle\langle k| . \tag{A7}$$

We will now calculate the shift of the atom-field state $|i,n\rangle$ due to couplings to other states $|s,m\rangle$ via H_{AF} and then use the properties of the coherent state to calculate the shift of our initial state $|i,\alpha\rangle$. The shift from second-order perturbation theory is

$$\Delta E_{i,n}=\sum_{s,m\neq i,n}\frac{|\langle s,m|H_{AF}|i,n\rangle|^2}{E_{i,n}-E_{s,m}} . \tag{A8}$$

The contribution of atomic state $|s\rangle$ to the sum is

$$\sum_m\left[\frac{eE_0}{2\sqrt{\bar{n}}}\right]^2\frac{|z_{is}\langle m|(a+a^\dagger)|n\rangle|^2}{\hbar[(\omega_i+n\omega)-(\omega_s+m\omega)]} . \tag{A9}$$

The first term ($\langle m|a|n\rangle$) requires $m=n-1$, which yields

$$\left[\frac{eE_0 z_{is}}{2}\right]^2\frac{1}{\bar{n}}\frac{n}{\hbar(\omega_{is}+\omega)} . \tag{A10a}$$

The second term ($\langle m|a^\dagger|n\rangle$) requires $m=n+1$, which yields

$$\left[\frac{eE_0 z_{is}}{2}\right]^2\frac{1}{\bar{n}}\frac{n}{\hbar(\omega_{is}-\omega)} , \tag{A10b}$$

where we have used $n+1\approx n$. Therefore we need only sum over atomic levels, and

$$\Delta E_{i,n}=\frac{1}{\hbar}\frac{e^2E_0^2}{4}\frac{n}{\bar{n}}\sum_{s\neq i}z_{is}^2\left[\frac{1}{\omega_{is}+\omega}+\frac{1}{\omega_{is}-\omega}\right] . \tag{A11}$$

With $\Omega_{is}\equiv eE_0 z_{is}/\hbar$ and $n\approx\bar{n}$,

$$\Delta E_{i,n}\approx\frac{\hbar}{2}\sum_{s\neq i}\frac{\Omega_{is}^2\omega_{is}}{\omega_{is}^2-\omega^2}\equiv\hbar\delta_i . \tag{A12}$$

Consequently, the constituent number states of the coherent state $|\alpha\rangle$ all have approximately the same Stark shift δ_i. They also all have approximately the energy of the coherent state $U_\alpha=(\bar{n}+\frac{1}{2})\hbar\omega$, and so we can identify δ_i as the frequency shift of the atomic state $|i\rangle$ in the presence of the radiation. The shift of the two-photon transition is

$$\delta_{if}=\left[\sum_{s\neq i}\frac{\Omega_{is}^2\omega_{is}}{2(\omega_{is}^2-\omega^2)}\right]-\left[\sum_{s\neq f}\frac{\Omega_{fs}^2\omega_{fs}}{2(\omega_{fs}^2-\omega^2)}\right] . \tag{A13}$$

The ac Stark shift of a one-photon transition cannot be evaluated from Eq. (A13) because the energy denominator is zero for $s=f$ when the radiation is resonant. The ac Stark shift can be calculated in the dressed basis [eigenstates of the full Hamiltonian, Eq. (A1)], but that calculation will not be presented here. The result has two parts: the shift of $|i\rangle$ due to states other than $|f\rangle$, which is given by Eq. (A13) with the sum restricted to $s\neq i,f$ where $|i\rangle$ and $|f\rangle$ are the initial (upper) and final (lower) states of the transition, and the shift due to level $|f\rangle$ (Bloch-Siegert shift), which is given by

$$\delta_i^{\mathrm{BS}}=-\delta_f^{\mathrm{BS}}=\frac{1}{4}\frac{\Omega_{if}^2}{\omega_{if}+\omega} . \tag{A14}$$

The Bloch-Siegert shift is due to the counter-rotating term that is neglected in the rotating-wave approximation.

[1]Claude Cohen-Tannoudji, Bernard Diu, and Franck Laloë, *Quantum Mechanics* (Wiley-Interscience, New York, 1977), Vol. 2, pp. 1339–1342.
[2]I. I. Rabi, Phys. Rev. **51**, 652 (1937).
[3]A. Abragam, *The Principles of Nuclear Magnetism* (Oxford University Press, Oxford, England, 1961).
[4]L. Allen and J. H. Eberly, *Optical Resonance and Two-Level Atoms* (Wiley, New York, 1975).
[5]Hiroshi Hatanaka and Tsuneo Hashi, J. Phys. Soc. Jpn. **39**, 1139 (1975).
[6]D. G. Gold and E. L. Hahn, Phys. Rev. A **16**, 324 (1977).
[7]Richard G. Brewer and E. L. Hahn, Phys. Rev. A **11**, 1641

(1975).
[8]D. Grischkowsky, M. M. T. Loy, and P. F. Liao, Phys. Rev. A **12**, 2514 (1975).
[9]D. Grischkowsky and Richard G. Brewer, Phys. Rev. A **15**, 1789 (1977).
[10]Axel Schenzle and Richard G. Brewer, Phys. Rep. **43**, 455 (1978).
[11]Philip Stehle, Phys. Rep. **156**, 67 (1987).
[12]H.-I. Yoo and J. H. Eberly, Phys. Rep. **118**, 239 (1985).
[13]Hiroshi Hatanaka, Toshiro Ozawa, and Tsuneo Hashi, J. Phys. Soc. Jpn. **42**, 2069 (1977).
[14]M. M. T. Loy, Phys. Rev. Lett. **41**, 473 (1978).
[15]P. F. Liao and J. E. Bjorkholm, Phys. Rev. Lett. **34**, 1 (1975).
[16]Michael G. Littman and Harold J. Metcalf, Appl. Opt. **17**, 2224 (1978).
[17]Winfried Hansen, J. Phys. B **16**, 2309 (1983).
[18]A. G. Vaidyanathan, W. P. Spencer, and B. J. Hughey (unpublished).
[19]M. M. Kash and G. R. Welch (private communication).
[20]Myron L. Zimmerman, Michael G. Littman, Michael M. Kash, and Daniel Kleppner, Phys. Rev. A **20**, 2251 (1979).
[21]Y. Kaluzny, P. Goy, M. Gross, J. M. Raimond, and S. Haroche, Phys. Rev. Lett. **51**, 1175 (1983).
[22]Gerhard Rempe, Herbert Walther, and Norbert Klein, Phys. Rev. Lett. **58**, 353 (1987).
[23]Barbara J. Hughey, Thomas R. Gentile, Theodore W. Ducas, and Daniel Kleppner, in *Proceedings of the Sixth Rochester Conference on Coherence and Quantum Optics,* edited by Leonard Mandel (Plenum, New York, in press); H. J. Kimble *et al., ibid.*
[24]J. J. Childs, M. Donovan, J. T. Hutton, F. W. Dalby, and M. S. Feld, in *Proceedings of the Ninth International Conference on Laser Spectroscopy,* edited by M S. Feld, A. Mooradian, and J. E. Thomas (Academic, New York, in press).
[25]M. Brune, J. M. Raimond, P. Goy, L. Davidovich, and S. Haroche, Phys. Rev. Lett. **59**, 1899 (1987).
[26]Rodney Loudon, *The Quantum Theory of Light,* 2nd ed. (Oxford University Press, Oxford, England, 1983), Chaps. 4 and 5. This reference provides the necessary background for the formalism used in this Appendix, however, we have chosen to expand the vector potential as $\mathbf{A} = i\,\mathbf{A}_k \exp(i\mathbf{k}\cdot\mathbf{r}) - i\,\mathbf{A}_k^* \exp(-i\mathbf{k}\cdot\mathbf{r})$ and have set $\exp(\pm i\mathbf{k}\cdot\mathbf{r}) = 1$.
[27]I. I. Sobel'man, *Introduction to the Theory of Atomic Spectra* (Pergamon, New York, 1972), p. 272. Though the expression for the ac Stark shift obtained in this reference is the same as Eq. (A15), the approach is not strictly applicable because of the large changes in the atomic populations associated with the Rabi oscillations.